AFRL-AFOSR-JP-TR-2024-0012

Gate-tunable and multifunctional metal nitride zero-index and plasmonic heterostructures for advanced optical sensing and energy harvesting

Zhenrong Zhang
BAYLOR UNIVERSITY
700 S UNIVERSITY PARKS DR
WACO, TX, 76706
USA

12/10/2023
Final Technical Report

Air Force Research Laboratory
Air Force Office of Scientific Research
Asian Office of Aerospace Research and Development
Unit 45002, APO AP 96338-5002

REPORT DOCUMENTATION PAGE

PLEASE DO NOT RETURN YOUR FORM TO THE ABOVE ORGANIZATION.

1. REPORT DATE	2. REPORT TYPE	3. DATES COVERED	
20231210	Final	START DATE 20180914	END DATE 20210913

4. TITLE AND SUBTITLE
Gate-tunable and multifunctional metal nitride zero-index and plasmonic heterostructures for advanced optical sensing and energy harvesting

5a. CONTRACT NUMBER	5b. GRANT NUMBER	5c. PROGRAM ELEMENT NUMBER
FA2386-18-1-4099		
5d. PROJECT NUMBER	**5e. TASK NUMBER**	**5f. WORK UNIT NUMBER**

6. AUTHOR(S)
Zhenrong Zhang

7. PERFORMING ORGANIZATION NAME(S) AND ADDRESS(ES)
BAYLOR UNIVERSITY
700 S UNIVERSITY PARKS DR
WACO, TX 76706
USA

8. PERFORMING ORGANIZATION REPORT NUMBER

9. SPONSORING/MONITORING AGENCY NAME(S) AND ADDRESS(ES)	10. SPONSOR/MONITOR'S ACRONYM(S)	11. SPONSOR/MONITOR'S REPORT NUMBER(S)
AOARD UNIT 45002 APO AP 96338-5002	AFRL/AFOSR IOA	AFRL-AFOSR-JP-TR-2024-0012

12. DISTRIBUTION/AVAILABILITY STATEMENT
A Distribution Unlimited: PB Public Release

13. SUPPLEMENTARY NOTES

14. ABSTRACT
The optical response of epsilon-near-zero (ENZ) materials has been a topic of significant interest in the last few years as the electromagnetic field inside media with near-zero permittivity has been shown to exhibit unique optical properties, including strong
electromagnetic wave confinement, non-reciprocal magneto-optical effects, and abnormal nonlinearity. These ultrathin ENZ materials are promising for the enhancement of quantum emission for optical sensing and enhanced absorption/emittivity for energy harvesting. While
ENZ optics have been extensively investigated in the last few years, the previous studies suffer from several limitations, including (i) lack of precise control of carrier distribution for efficient ENZ mode excitation, (ii) lack of efficient tunability due to the fixed conductivity of
the noble metal/semiconductor, (iii) high optical loss due to the amorphous or high surface roughness of the film, and (iv) narrow bandwidth of operating wavelength (<10 nm). Until we can solve these problems and manipulate and enhance the zero-index optical dynamic, we cannot develop efficient nanoscale ENZ optical applications for quantum optical sensing and energy harvesting. The objective in this collaborative research project is to establish an efficient material and electrical management of the enhanced optical properties, such as quantum emission, optical phase and absorptivity/emissivity, of metal nitride zero-index and
plasmonic heterostructures for nano-optoelectronic devices.

15. SUBJECT TERMS

16. SECURITY CLASSIFICATION OF:			17. LIMITATION OF ABSTRACT	18. NUMBER OF PAGES
a. REPORT	b. ABSTRACT	c. THIS PAGE	SAR	20
U	U	U		

19a. NAME OF RESPONSIBLE PERSON	19b. PHONE NUMBER *(Include area code)*
JEREMY KNOPP	315-227-7006

Standard Form 298 (Rev.5/2020)
Prescribed by ANSI Std. Z39.18

Howard Lee, Zhenrong Zhang, Baylor University
AFOSR-MOST Program

Grant # FA2386-18-1-4099

AFOSR
Final Report

Period Covered by the Report: September 14, 2018 through September 13, 2021
Date of Report: December 10, 2021
Lead Organization: Baylor University, USA; University of California, Irvine; National Tsing-Hua University, Taiwan
Technical Point of Contact:
Howard Lee
Department of Physics & Astronomy, University of California, 4129 Frederick Reines Hall, Irvine, CA 92697-4575
Email: Howardhw.lee@uci.edu
Department of Physics, Baylor University, One Bear Place #97316, Waco, TX 76798-7316
Telephone: 254-710-2277
Email: Howard_Lee@Baylor.edu

Zhenrong Zhang
Department of Physics, Baylor University, One Bear Place #97316, Waco, TX 76798-7316
Telephone: 254-710-2419
Email: Zhenrong_Zhang@baylor.edu
Administrative POC:
Kristy Erlanson
Street Address: One Bear Place #97360, Waco, TX 76798-7360
Phone: 254-710-8608
Email: Kristy_Erlanson@baylor.edu
Project Title: Gate-tunable and multifunctional metal nitride zero-index and plasmonic heterostructures for advanced optical sensing and energy harvesting
Total Dollar Value: $ $299,001
Most relevant BAA Section: Novel multifunctional materials
AFOSR Program Manager: Dr. Jeremy Knop

1. Accomplishments:

1.1. Research Objective:

The ***objective*** in this collaborative research project is to establish an efficient material and electrical management of the enhanced optical properties, such as *quantum emission*, *optical phase* and *absorptivity/emissivity*, of metal nitride zero-index and plasmonic heterostructures for nano-optoelectronic devices. In addition, we plan to utilize our collaborative nanophotonic research and infrastructure to provide the undergraduate and graduate students at Baylor University in the US and National Tsing-Hua University in Taiwan with exposure to the collaborative environment, the required nanophotonic skills and knowledge, and the international exchange opportunities that are important for their future academic and industrial careers.

The research program focuses on the following three ***specific tasks***:

1. **Establish broadband enhancement of quantum emission with MBE-grown TiN ENZ meta-film for quantum optical sensing.** *We will develop low loss, single crystalline, and ultrasmooth TiN ENZ materials with precise control of the carrier distribution spatially using the MBE technique.* The enhanced and broadband ENZ mode excitation will be used to enhance Raman emission for optical sensing and energy harvesting.
2. **Identify and enhance the excitation of TiN ENZ resonances in gate-tunable ENZ metasurface heterostructures for enhanced quantum optical emission.** *We will investigate new tunable coupled resonant ENZ metasurface nanostructures to establish efficient quantum emission and optical phase modulation in the visible and NIR spectrum.* The controllable enhanced ENZ field confinement and phase will further advance the optical sensing ability through surface enhanced Raman spectroscopy (SERS) and surface enhanced coherent anti-stokes Raman spectroscopy (SECARS).
3. **Examine the broadband emissivity/absorptivity with TiN ENZ materials for energy h arvesting**. We aim to develop control of selective thermal emissivity and broadband abs orption through the use of TiN gradient ENZ nanolayers and metasurfaces fabricated by MBE/ALD and field-effect electrical gating techniques.

1.2. Research Accomplishment:

During the program, Lee/Zhang groups have experimentally and numerically investigated novel ENZ excitation platforms and materials to enhance, to tune, and to integrate the zero-index properties such as enhanced emission and absorption of epsilon-near-zero (ENZ) media. We have developed techniques to fabricate TiN thin film with single or double ENZ properties. The following is a list of major accomplishments of project's objectives:

- Demonstrated enhanced photoluminescence properties of MoS2 monolayers on titanium nitride (TiN) thin films grown on sapphire by molecular-beam-epitaxy (MBE). We observed photoluminescence enhancement increases as TiN becomes more metallic and an order of magnitude enhancement is obtained at the excitation wavelengths 488 nm and 561 nm.
- Investigated photoluminescence enhancements between different sputtered and MBE grown TiN samples and different oxide thicknesses.
- Developed fabrication techniques to fabricate high quality single crystalline TiN through the molecular beam epitaxy (MBE), magnetron sputtering, atomic layer deposition (ALD) technique. We were able to control the single and double ENZ properties and wavelength in the visible region.
- Demonstrated broadband absorption at high temperature in TiN plasmonic metasurfaces.
- Demonstrated plasmonic perfect absorbers using a titanium nitride metasurface.

Enhanced Spontaneous Emission of Monolayer MoS2 on Epitaxially Grown Titanium Nitride Epsilon-Near-Zero Thin Films

Room temperature photoluminescence enhancement of molybdenum disulfide (MoS_2) monolayers on epitaxial titanium nitride (TiN) thin films grown by molecular-beam-epitaxy as well as magnetron-sputtered TiN films is observed by a confocal laser scanning microscope with excitation wavelengths covering the transition of TiN's macroscopic optical properties from dielectric to plasmonic. The photoluminescence enhancement increases as TiN becomes more metallic, and strong enhancement is obtained at the excitation wavelengths equal to or longer than the epsilon-near-zero (ENZ) wavelength of TiN films. A good agreement is observed between measured and calculated enhancements. The enhancement is attributed to the increased excitation field in MoS_2 at TiN's ENZ wavelength, and interference effects for thick spacers that separate the MoS_2 flakes from TiN films in the metallic regime.

To investigate the emission properties on ENZ media, the photoluminescence (PL) from MoS_2 flakes on thin (~50 nm) and thick (~120 nm) TiN films, is measured using a confocal laser scanning fluorescence microscope with several excitation wavelengths, namely 405, 445, 488 and 561 nm. The measured PL enhancement, the ratio of integrated PL intensity with TiN substrate to that with reference sapphire substrate, is verified against the PL enhancement modelled by means of rigorous luminescence calculation methods. To gain insight into the role of optical losses in the PL enhancement of ENZ films fabricated with different methods, we also compare the PL enhancements of TiN films grown by molecular beam epitaxy (MBE) and magnetron sputtering methods (Fig. 1b,c). To reduce non-radiative recombination of excitons, an alumina spacer layer of a few nanometers separates the MoS_2 layer and TiN substrates.

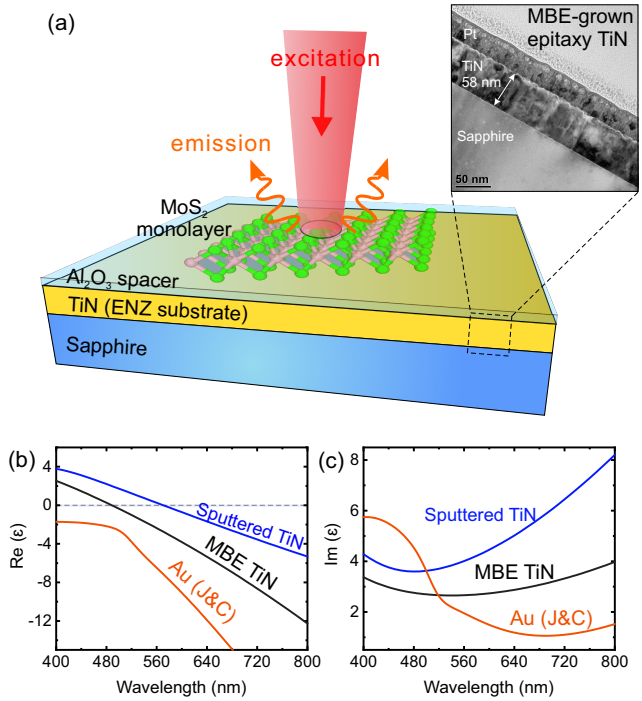

Fig. 1: (a) Schematic of the structures for studying spontaneous emission on TiN ENZ substrate. Inset: TEM image for one of the MBE-grown epitaxial TiN samples with thickness of 58 nm. The platinum (Pt) layer is deposited on TiN to avoid the issue of charging during the sample preparation for the TEM imaging.. (b) Real and (c) Imaginary part of permittivity of MBE-grown single-crystalline TiN film (thickness 133 nm) and sputtered TiN film (thickness 146 nm) measured from spectroscopic ellipsometry and gold from literature.

The assembly of emitter and substrate layers used in the experiment is sketched in figure 2a. It consists of c-sapphire substrate, epitaxial (sputtered) TiN films, atomic layer deposited Al_2O_3 spacer layer and MoS_2 monolayer flakes. The spacer is not included in the reference sample that consists of MoS_2 flakes on c-sapphire substrate. The PL images are taken with dry 0.9 NA objective at normal incidence. A typical PL map integrated from 640 to 700 nm emission wavelength obtained by 561 nm excitation of the flakes on epitaxial TiN and on reference sapphire are shown in figure 2b. The two maps have the same greyscale for direct comparison and emission of MoS_2 on TiN is clearly much brighter than on sapphire. In addition, the PL enhancement on titanium nitride with respect to sapphire depends on the excitation laser wavelength, as shown in the emission spectra plotted in figure 2c for four excitation wavelengths.

Room temperature PL spectra of MoS_2 flakes on both substrates have neutral A and B exciton peaks and charged exciton A^- trion peak, which shapes are descried by Lorentzian functions (figure 2c) [1]. The excitonic peak wavelengths decrease slightly as the excitation wavelength increases.

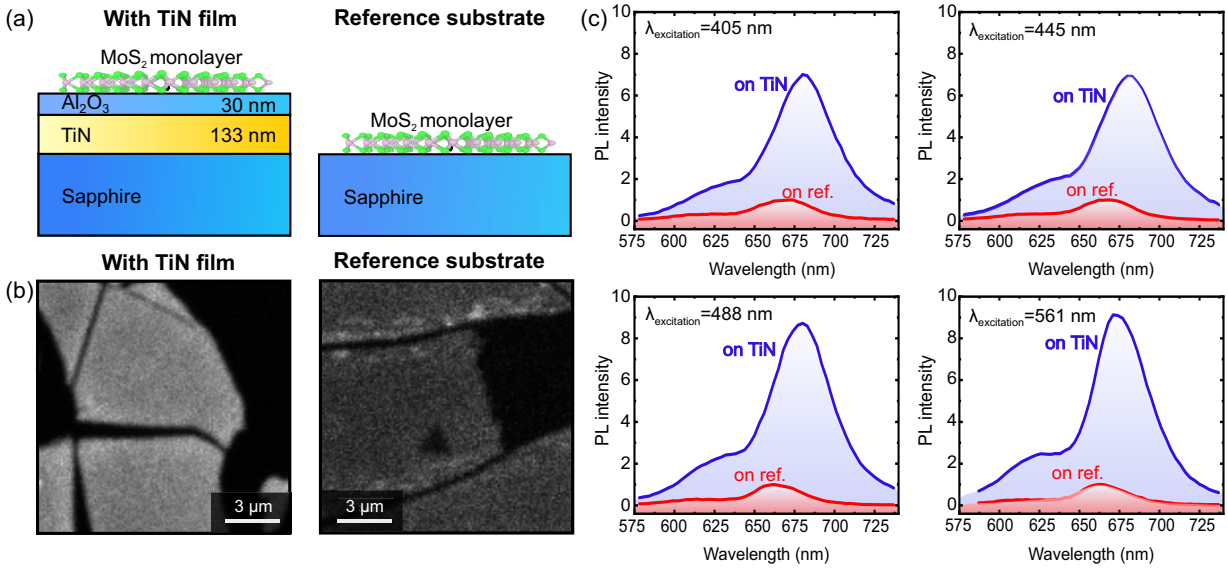

Figure 2. Photoluminescence measurements. (a) Schematics of the samples. (b) Typical photoluminescence maps of MoS_2 on titanium nitride substrate and sapphire substrate. The scale bar is 3 μm. (c) PL spectra of MoS_2 using four different excitation lasers.

To gain insight into the dependence of the PL enhancement on excitation laser wavelength, we performed numerical calculations of fluorescence enhancement for an emitter embedded inside a multilayer geometry.[2, 3] The total electromagnetic enhancement is the product of two contributions: excitation enhancement and emission enhancement.[3, 4] The excitation field enhancement due to the 120 nm thick TiN substrate leads to enhanced absorption of MoS_2 normalized with respect to the reference sample (see Eq. **Error! Reference source not found.**), which varies with spacer thickness and excitation wavelength (figure 3a). In this configuration, TiN film acts as a reflector; the field intensity and consequently the absorptance is enhanced due to interference of the incident and reflected beams inside the open cavity. For spacer thicknesses comparable to the quarter of the incident wavelength or larger, the multi-beam interference dominates and the Fabry-Perot resonances are responsible for the large enhancements.

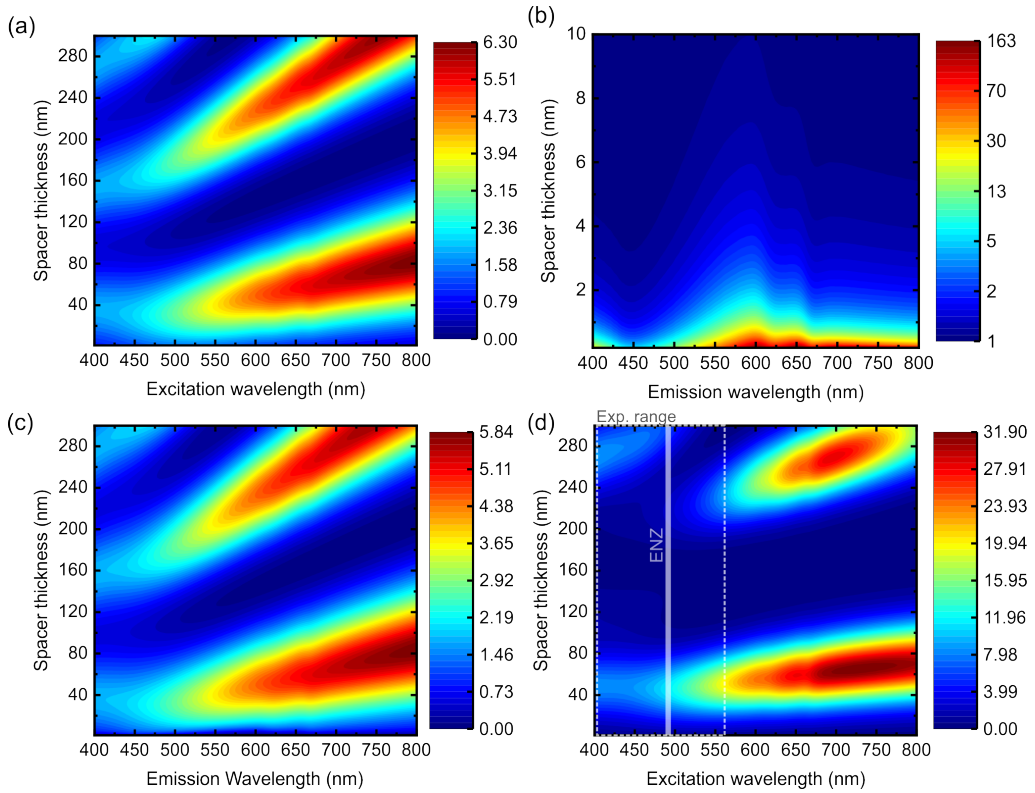

Figure 3.(a) Absorption enhancement of MoS_2 on titanium nitride with respect to sapphire (b) the Purcell factor (c) quantum efficiency enhancement and (d) total electromagnetic enhancement of in-plane dipole in MoS_2 monolayer on titanium nitride as a function of spacer thickness.

The emission enhancement due to TiN substrate with respect to the sapphire substrate at the emission wavelength is the enhancement in the radiative quantum efficiency which is defined as a fraction of the radiative decay rate modified by the Purcell factor to the total decay rate, and which depends on the intrinsic quantum efficiency.[2-4] The Purcell factor, which includes decay rate into far-field, surface modes and absorption in the metal, of an in-plane dipole located in the middle of MoS_2 layer above 120 nm thick TiN is calculated as a function of emission wavelength and spacer thickness (figure 3b). Purcell factor is greatly enhanced for small spacer thicknesses due to the high local density of optical states near the metallic TiN surface at the MoS_2 excitonic emission wavelengths. External quantum efficiency enhancement has similar spacer dependence to the absorption enhancement for spacers larger than ~10nm (figure 3c). In this thickness range, Purcell enhancement is negligible, and the emission enhancement is due to the interference effects. Total electromagnetic enhancement at the 660 nm emission wavelength is plotted in figure 3d. The maximum enhancements are experientially unattainable since the excitation wavelength for maximum enhancement overlap with the emission wavelength range. The experimentally attainable enhancements inside the dashed box shows the open cavity resonance around ~30 to ~50 nm spacer range and Fabry-Perot resonances for the large spacers.

Experimental demonstration of photoluminescence enhancement of MoS2 monolayers on TiN ENZ substrate for aluminum oxide thickness of 30 nm.

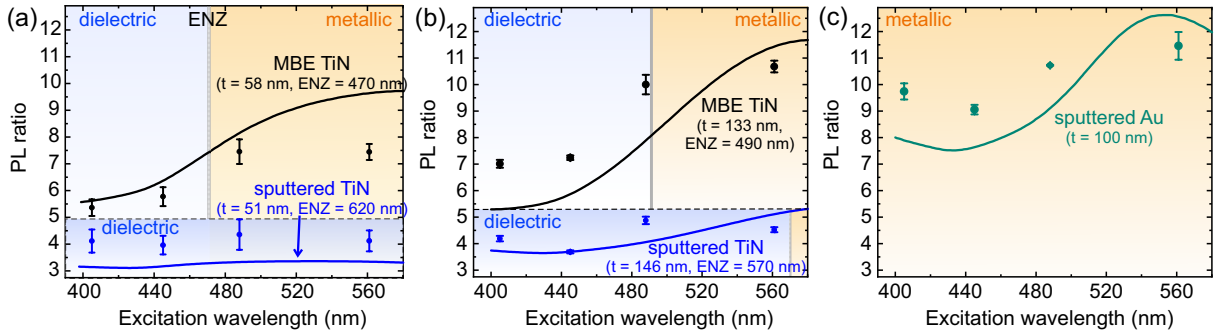

Figure 4. Experimental and calculated PL enhancements of MoS_2 on TiN and Au substrates with 30 nm spacer with respect to sapphire substrate. Substrates are (a) 58 nm thin epitaxial TiN and 51 nm thin sputtered TiN, (b) 120 nm thick epitaxial TiN and 146 nm thick sputtered TiN (c) 100 nm thick sputtered Au. Gray and blue vertical lines indicate the ENZ wavelengths of MBE films and sputtered films respectively.

In the experimental results plotted in figure 4, spacer thickness of 30 nm is used to compare the open cavity resonance of epitaxial TiN, sputtered TiN and sputtered gold films in the thin (~50 nm) and thick (~120 nm) film regimes. Experimental PL enhancement as a function of excitation wavelength shows good agreement with the calculated enhancements. As TiN transition from lossy dielectric to metallic across the ENZ wavelength, the PL enhancement becomes stronger. The MBE-grown TiN films, having ENZ at smaller wavelengths as well as lower optical losses across the visible and IR spectrum, enhance PL emission by 2 to 3 times greater than sputtered films (black vs blue curves in figure 4a and 4b). Among the two MBE films, the PL enhancement for 120 nm thick TiN is larger than the 58 nm sample due to smaller loss and higher reflectivity (black curves in figure 4a vs 4b). Interestingly, it can be observed that epitaxial TiN and Au have comparable performance (black curves in figure 4b vs 4c), especially above the ENZ wavelength of TiN where its negative real permittivity gets larger and more metallic. In the dielectric domain, TiN have relatively smaller enhancement than Au despite having smaller loss, which is expected in this open-cavity regime because the emitter is far enough from the lossy medium that the contributions by the surface modes and metal absorption is insignificant.

Experimental demonstration of photoluminescence enhancement of MoS2 monolayers on TiN ENZ substrate for aluminum oxide thicknesses < 10 nm.

For thin spacers, far away from the geometrical resonances, maximum field and absorption enhancements (figure 5a) are determined by the material property of TiN. PL enhancement is optimal at the excitation wavelengths near the maximum absorption due to ENZ wavelengths (cf. Eq. **Error! Reference source not found.**). Despite exponentially growing Purcell factor (figure 5b), the external quantum efficiency enhancement decreases (figure 5c), as the spacer thickness is decreased. Hence it can be deduced that the decay rate into surface modes and metal absorption dominates. The peak in the Purcell factor for ultrathin (< 5 nm) films is at the surface plasmon resonance, red-shifted from the ENZ wavelength as indicated by the band-structure calculation. In contrast to the open-cavity and Febry-Perot resonances, the maximum PL enhancement (Figure 5d) is within experimentally attainable range inside the dashed box. The experimental PL enhancement (Figure 5e and 5f) as a function of excitation wavelength slightly differs from the calculated enhancements. Intrinsic quantum efficiency (IQE) of 0.004 is used in the calculation.[5] This small deviation for thin spacer can be attributed to the uncertainty in the spacer thickness and the variation in the IQE q0 of monolayer MoS_2 whose effect is pronounced in proximity to the absorbing medium. However, the dependence on the excitation wavelength observed in the experiments is replicated by the calculations.

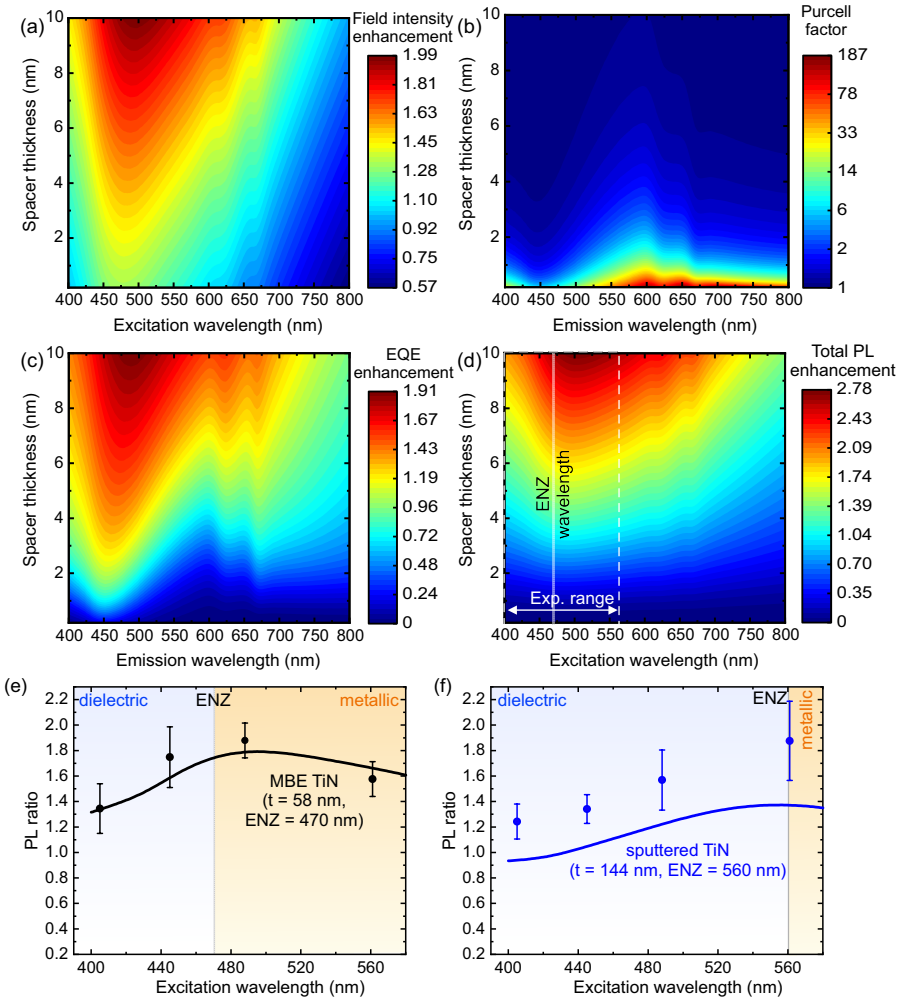

Figure 5. (a) Field intensity enhancement inside MoS_2 on titanium nitride with respect to sapphire (b) the Purcell factor (c) quantum efficiency enhancement and (d) total electromagnetic enhancement of in-plane dipole in MoS_2 monolayer on titanium nitride (thickness 58 nm) for thin spacers (e,f) Experimental PL enhancement of MoS_2 on MBE-grown (e), and sputtered (f) TiN substrates with respect to that on sapphire substrate. The calculated enhancement (lines) is shown for several spacer thicknesses and a fixed intrinsic quantum efficiency of 0.4%.

We expect the emission enhancement of TiN to find widespread applications. In particular, the ultrathin epitaxial crystalline TiN films can switch from a poor (dielectric) to good (metallic) reflector with applied voltage at a fixed wavelength in the visible range due to the electrically tunable permittivity of the films. This property may be of great importance to various optical, optoelectrical, display, and energy harvesting technologies which align with the focuses of this project.

Controllable single and double epsilon-near-zero properties in titanium oxynitride materials fabricated with sputtering technique.

We have fabricated TiN ENZ materials with MBE technique (in collaboration with Taiwan counterpart). The most significant feature is that, unlike noble metals such as gold, TiN transitions from dielectric to metallic in the visible spectrum with the ENZ crossing wavelength at 490 nm for MBE-grown film and 570 nm for sputtered film. In addition, the TiN films have similar loss as gold in the visible regime (Fig. 1b, c). The MBE-grown TiN permittivity has both larger real part $|\varepsilon'|$ and smaller imaginary part ε'', implying better plasmonic performance, than the sputtered sample.

However, the MBE grown TiN exhibit short ENZ wavelength ~ 490 nm, and the MBE technique is difficult to tune the ENZ wavelength to longer wavelength due to the high carrier concentration of samples.

Therefore, we investigated the fabrication of TiN with sputtering technique. We explore a different method of magnetron sputtering of TiN and TiON compared to the previously reported magnetron sputtering method of TiON. The previous report of TiON was made using a 99.999% pure Ti target while we used a 99.5% TiN [6-10]. For the characterization of the optical properties of the resulting thin films, we measured them using ellipsometry. The use of a TiN target compared to the Ti target simplifies the deposition of these films because of the parameter of the nitrogen gas percentage is removed. The only parameters left that need to be focused on then are residual oxygen and water vapor pressure, temperature, and deposition pressure of the films.

The residual oxygen and water vapor pressure are the hardest of the three parameters to control and it also has a huge impact on the resulting TiN. The more of these residual gases are left in the chamber allows for more oxygen to combine into the film to form TiO_x and TiO_xN_y within the film which results in the film being more towards dielectric. If enough of these residual gases are left in the chamber allows for more oxygen to combine into the film to form TiOx and TiOxNy within the film which results in the film being more towards dielectric. If there are too many of these residual gases left into the chamber the film will be completely dielectric. For this setup of deposition pressure at 5 mTorr and a temperature of 400°C this transition point can be estimated to be around 6 to 6.5 mTorr depending on the residual water vapor. The effects of residual oxygen and water vapor pressure are shown in figure 6. In figure 6 the samples are deposited at a temperature of 400°C, a deposition pressure of 5 mTorr of Argon (Ar) gas, and a thickness of about 60 nm. The resulting film with 7.32 nTorr of residual oxygen pressure was completely dielectric and as this decreases the film then can go into the double ENZ range. This can be seen with the other films that have 4.01-5.43 nTorr of residual oxygen pressure. If the residual oxygen can be reduced even further then single ENZ films can be produced but due to limitations of our sputtering machine these residual pressures cannot be obtained. It can be seen that the resulting films can be reproduced as shown with the two samples that are deposited at 5.43 nTorr but the residual water vapor pressure is slightly different which does lead to some changes in the film but there double ENZ are the same within measurement uncertainties. It can also be seen that there is both a blue shifting of the double ENZ properties and a boarding between these two ENZ values of these films as the residual oxygen is reduced. The first ENZ region of these thin films gets shifted from 1025-1150nm to 900-1000nm and the second region is shifted from 1300-1400nm to 1100-1180nm.

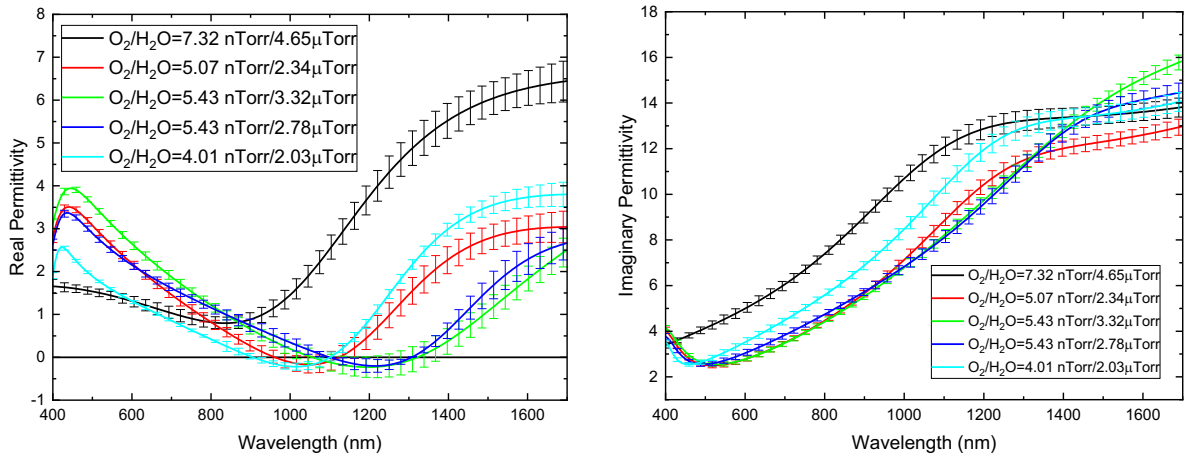

Figure 6. Real and imaginary parts of permittivity with varying residual oxygen and water vapor pressure while keeping deposition temperature at 400°C and deposition pressure at 5 mTorr.

Figure 7 shows the deposition temperature effects on the deposited films. The residual partial pressure measurements are unreliable because of has heat is increased or decreased so will the pressure increase or decrease. To be able to resolve this issue a deposition procedure was used to maintain similar environments so that there should be little differences between the samples like the reproducible results in figure 6. In Figure 7 we can see decreasing the deposition temperature results in the films being more dielectric which causes the double ENZ to red-shift and narrowing the difference between the double ENZ. The temperature of deposition can be used to control how much residual oxygen and water vapor can combine into the resulting film because the extra energy makes it more difficult for the bonds of TiON to form. If this is combined the effects of changing the residual oxygen and water vapor to have more control over the optical properties of these resulting films.

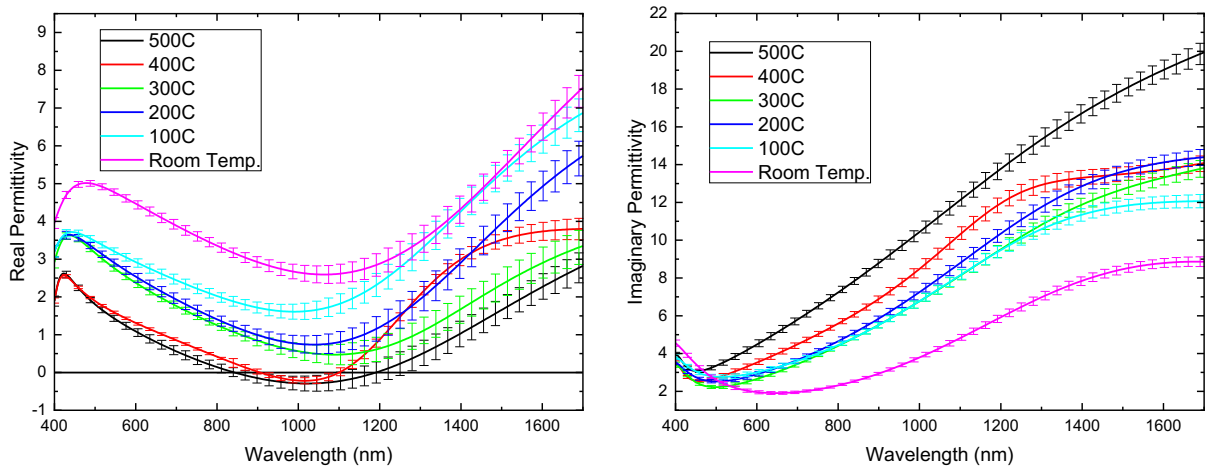

Figure 7. Real and imaginary parts of permittivity with varying deposition temperature while while keeping a fixed process for residual oxygen and water vapor pressure and deposition pressure at 5 mTorr.

Figure 8 shows the effects of deposition pressure on the deposited films. It can be seen that decreasing the deposition pressure of Ar gas that the films become more metallic and allow for single ENZ films. The lower the deposition the less likely that the oxygen can form bonds to make TiON because of the reduced amount of oxygen ions that are formed which will cause it to be less likely to form a bond with the Ti and TiN deposited. The range achieved in single ENZ thin films is from 500-800nm and combined with the effects of temperature and residual gases could allow for control over the optical properties of these films. The single ENZ could be controlled within this range and also the possibility of a larger range than what is demonstrated while keeping the other parameters relatively constant. We are currently investigating to use these TiN ENZ samples for the measurement of enhanced emission, absorption, and optical nonlinearity.

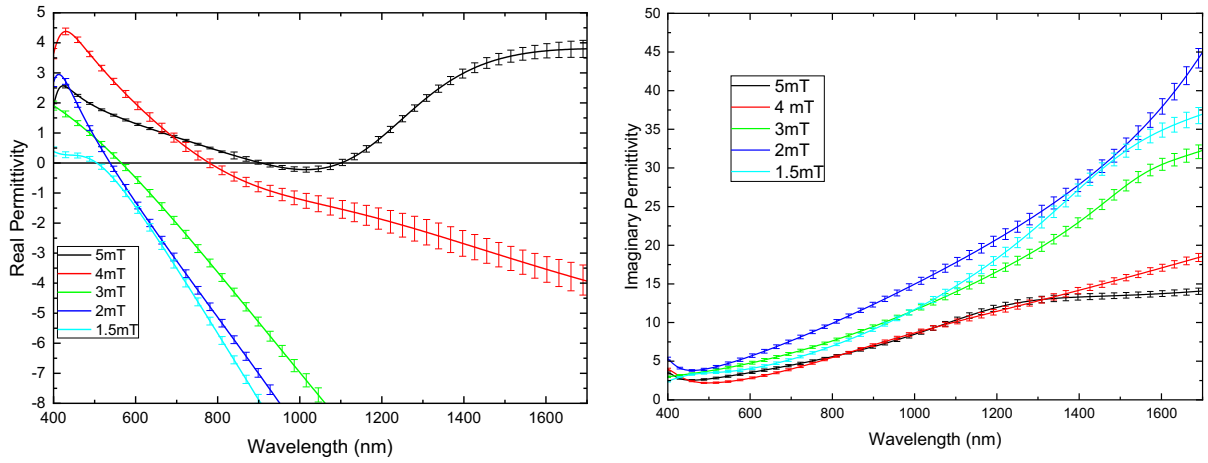

Figure 8. Real and imaginary parts of permittivity with varying deposition pressure while keeping a fixed process for residual oxygen and water vapor pressure and deposition temperature at 400°C.

Optimized Titanium Nitride Plasmonic Metasurface for Optical Broadband Absorption at High Temperature

TiN plasmonic metasurfaces have been applied as optical broadband absorbers and narrowband thermal emitters, which are critical for high-efficiency solar thermophotovoltaics. In this work, we demonstrate that a single-layer metasurface structure made from the oxidation-resistant TiN(111) epitaxial film grown on c-plane sapphire by molecular-beam epitaxy (MBE) can function as a broadband absorber with ~90% absorptivity over the visible spectrum. This is accomplished by optimized plasmonic characteristics of oxygen-free stoichiometric TiN films grown by MBE, in comparison with TiO_xN_y films prepared by the reactive sputtering technique. In addition, the excellent thermal and chemical stabilities of MBE-grown TiN metasurface are confirmed by vacuum annealing at 850 °C and irradiation under 130 suns in the ambient environment.

In this study, the (111)-oriented TiN epitaxial film (~200 nm thick) with a close-packed, rock-salt crystal structure is grown on a 2-inch (0001)-oriented (c-plane) sapphire wafer and *in-situ* streaky reflection high-energy electron diffraction (RHEED) patterns during and after the growth process indicate the smooth crystalline nature of the MBE TiN film. In comparison to (001) and (110) orientations, a recent study has demonstrated that the (111)-oriented TiN is more resistant to oxidation, even under a high oxygen partial pressure at 800 °C. To compare with the oxygen-free stoichiometric film grown by MBE, a sputtered (111)-oriented TiN epitaxial film is also prepared by reactive sputtering on c-plane sapphire and the same metasurface structure is used for a direct comparison. As a simple inspection method, the absence or presence of oxygen contamination can be judged by the film color and carrier concentration. The MBE TiN film exhibits a brilliant golden color, as shown in Fig. 8a, and has a free electron concentration as high as 9×10^{22} cm^{-3}. The dielectric functions (permittivity) of MBE and sputtered TiN films shown in Fig. 9c,d are measured by spectroscopic ellipsometry (SE) and fitted by using the Drude-Lorentz model.

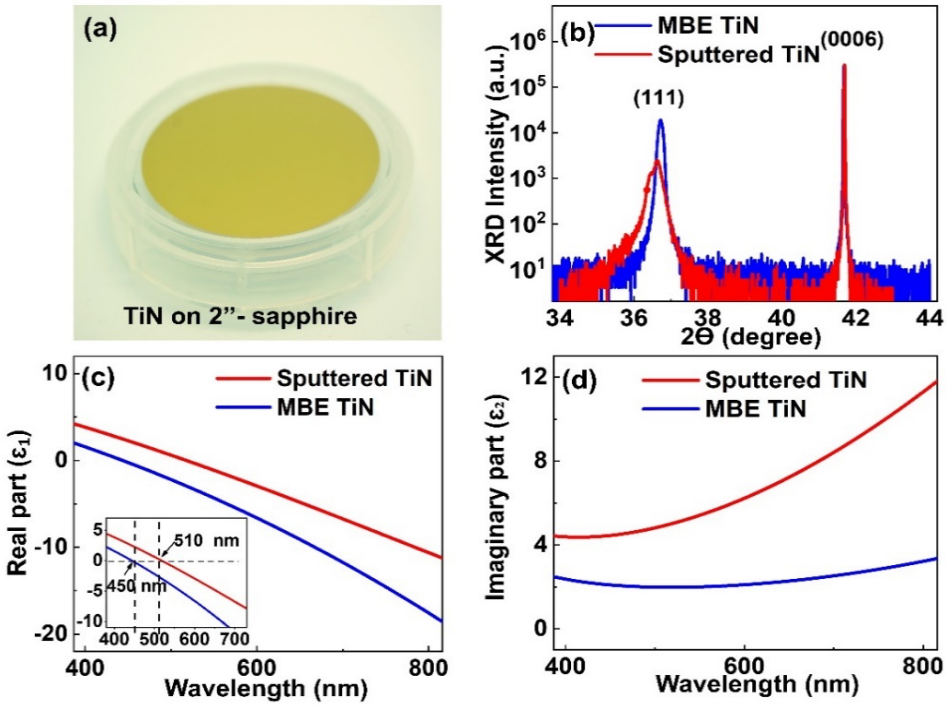

Figure 9. Comparison of optical properties measured for TiN epitaxial films grown by MBE and reactive sputtering on c-plane sapphire substrates. (a) Gold-film-like optical image of TiN epitaxial film grown by MBE with a film thickness of 200 nm. (b) X-ray diffraction patterns (X-ray wavelength: 1.54 Å) show the MBE TiN (111) peak at 36.7° and the sputtered TiN (111) peak at 36.5° with respect to the c-plane sapphire (0006) peak at 41.7°. (c, d) The dielectric functions (ε_1 and ε_2) of TiN films measured by spectroscopic ellipsometry for MBE and sputtered TiN films. According to the SE data, the crossover (ε_1 = 0) wavelength occurs at λ = 450 nm for the MBE TiN film and the λ = 510 nm for the sputtered TiN film. The value of imaginary part (ε_2) measured for the MBE TiN film in the wavelength range of 400–800 nm indicates that it has a lower optical loss.

Herein, we demonstrate the TiN metasurface broadband absorber for high temperature applications. In Fig. 10a, the single-TiN-layer metasurface structure is schematically shown. The nanohole array structure is chosen because of its simplicity and good performance. Moreover, the single-TiN-layer metasurface requires a less complicated fabrication process, as compare to the common metal insulator metal (MIM)-based perfect absorber. On such a array, nanoholes are periodically distributed in both *x* and *y* directions with specifically designed hole pitch, diameter, and depth for optimized broadband absorption over the full visible spectral region. Figure 3b shows the scanning electron microscope (SEM) image of the actual TiN metasurface fabricated by electron beam lithography. This TiN metasurface absorber is polarization independent at normal incidence of incident light. The perfect ("dark") absorber nature of the TiN metasurface is shown in the inset of Fig. 10b, which is an optical microscope image using an unpolarized white light.

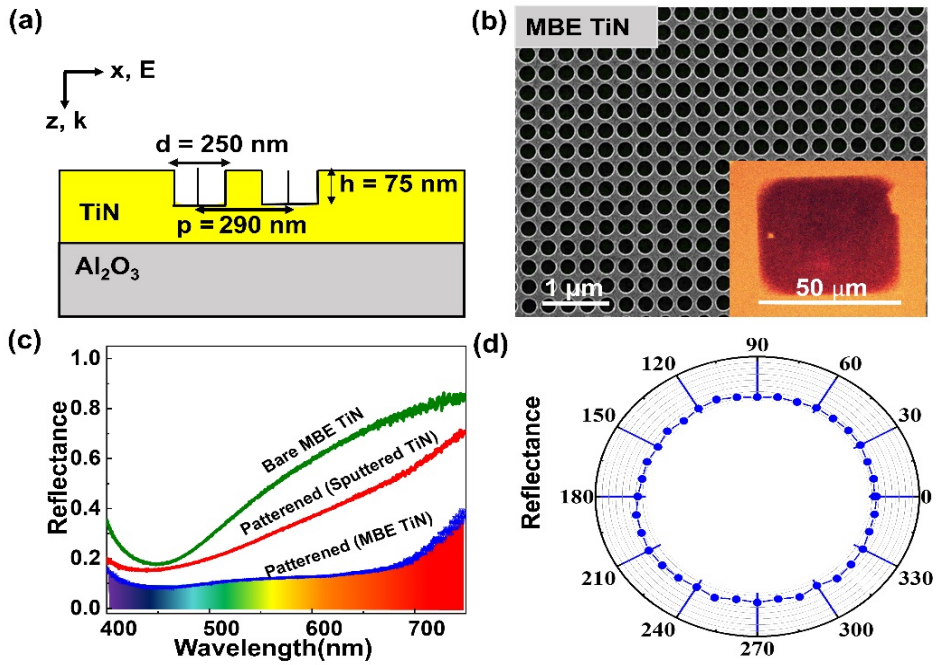

Figure 10. TiN metasurface solar absorber. (a) Schematic representation of the absorber consisting of a TiN nanohole array with optimized structural parameters: pitch (*p*) = 290, diameter (*d*) = 250 nm, height (*h*) = 75 nm. The MBE-grown TiN epitaxial film was grown on a sapphire wafer with a film thickness of 200 nm. (b) SEM image of the TiN nanohole array and the insect shows an optical microscope image of the nanohole array, demonstrating a strong absorption in the full visible range. (c) Comparison spectra of optical absorbance measured for the MBE TiN metasurface (blue), the sputtered TiN metasurface (red) using the same nanoholes array structure, and a bare MBE TiN film (green). (d) Polarized reflectance plot measured for the MBE TiN metasurface confirms that the broadband optical absorption is insensitive to the incident light polarization.

In comparison, we measure reflectance spectra (Fig. 10c) of as-fabricated metasurfaces made from MBE and sputtered TiN films, as well as a bare MBE TiN film. The absorbance (*A*) of metasurface can be derived from 1–*R*, where *R* is the reflectance since transmittance is zero due to the absorbing nature of the metallic film with a sufficient thickness. This assumption when the wavelength is shorter than the crossover wavelength (~450 nm for the MBE TiN film) as the film is no longer metallic, as shown in Fig. 10c for the case of bare MBE TiN film (green curve). In Fig. 3C, the blue curve represents experimental reflectance spectra of MBE TiN metasurface, where the absorption is ~90% over the visible range. By contrast, the sputtered TiN metasurface shows a lower absorption (the red curve) due to the oxidized nature of sputtered TiN confirmed by XPS analysis. Figure 10d shows a polarized reflectance plot measured for the MBE TiN metasurface, confirming that optical absorption is insensitive to the incident light polarization.

A demanding high-temperature, oxidation-resistant operation is compulsory in order to conclude their suitability for STPV applications, which require highly concentrated sunlight. The concentrated sunlight is converted into heat and the local heating effect can cause material damage before the average temperature reaches to the melting point of TiN metasurface. To evaluate the stable performance of TiN metasurface absorber, we use a solar simulator at different irradiation intensities of 70 suns (7 W/cm^2), 90 suns (9 W/cm^2), and 130 suns (13 W/cm^2) in a wavelength range of 400–1,200 nm. And the MBE and sputtered TiN metasurface absorbers are exposed to the solar simulator in the ambient environment at these irradiation intensities for

6 hours. Notably, the stoichiometric MBE TiN metasurface absorber can progressively tolerate the sun irradiation up to 13 W/cm^2 (130 suns) for 6 hours, as shown in the Fig. 11a. In contrast, the sputtered TiN absorber starts to be damaged when irradiation reach an intensity of 13 W/cm^2 (130 suns).

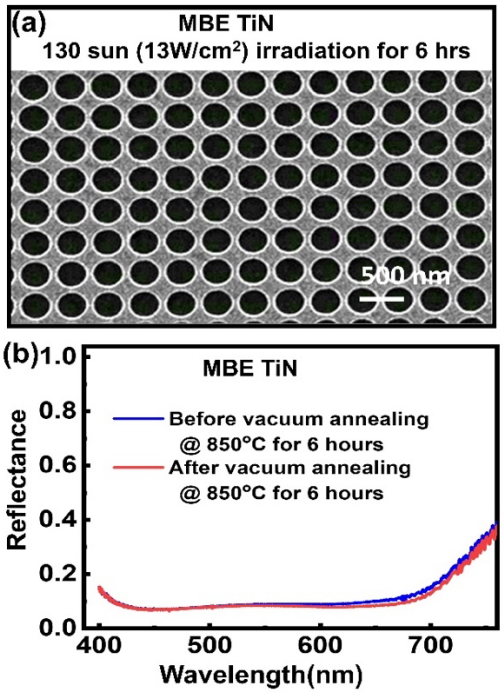

Figure 11. Thermal stability of the MBE TiN broadband absorber. (a) SEM image of the MBE TiN absorber under sun irradiation at an intensity of 130 suns (13 W/cm²) for 6 hours. (b) Measured absorption spectra of the MBE TiN absorber before and after vacuum annealing at 850°C for 6 hours.

In addition, we have also examined the thermal stabilities of two different TiN absorbers. For this purpose, we heat the MBE and sputtered TiN metasurface absorbers in an ultra-high vacuum chamber at three temperatures (600, 700, and 850 °C) for 6 hours. In this experiment, the MBE and sputtered TiN absorbers retain their morphology and optical performance after annealing at 600 and 700 °C. However, after both metasurfaces are heated at 850 °C or 6 hours, major differences start to appear. While there is no change for the case of MBE TiN metasurface absorber, as demonstrated in Fig. 11b, the sputtered TiN metasurface absorber has a drastic morphology change and the optical properties also seriously affected. This is likely due to the significant oxygen content in the sputtered TiN film, which can seriously degrade the thermal stability.

In this work, we show that the MBE TiN epitaxial film exhibits excellent thermal and chemical stabilities under high-temperature annealing in vacuum and high solar irradiance, which make it a promising material for demanding high-temperature applications such as solar thermophovoltics.

Plasmonic perfect absorbers using a titanium nitride metasurface.

In this work, we theoretically and experimentally demonstrate that a titanium nitride plasmonic metasurface absorber exhibits broadband perfect absorption with an average absorption of more than 92 % over a broad wavelength range of 400 nm to 750 nm. The increase in absorption is mainly attributed to the local-electromagnetic-field-enhanced light-matter interaction. We

demonstrate the plasmon-enhanced visible-light-driven production of hydrogen production from water using a polymer photocatalyst integrated with a TiN metasurface. A 200 % increase in the hydrogen evolution rate was observed because of the broadband localized-surface-plasmon resonance of the plasmonic TiN nanodisk arrays. These results enable a new approach to prepare solar energy harvesting devices.

Our design of a refractory nearly perfect absorber consists of a bottom layer TiN film with TiN nanodisk arrays directly conjoined on top. As shown in Fig.12a, the pattern of the square-arrangement array of nanodisks was defined by electron beam lithography and dry etching (see Sample Fabrication). The upper layer is TiN nanodisk arrays with a pitch (P) of 310 nm, a diameter (D) of 210 nm, and a thickness (h_2) of 110 nm in one unit cell; the conjoint bottom layer is a TiN film with a depth (h_1) of 50 nm. The symmetry of the periodic nanodisks makes the absorber polarization independent. The scanning electron microscopy (SEM) image in Figure 12b reveals TiN nanodisk arrays as well as apparent grains in those areas excluding nanodisks. These grains originate from damage due to the dry etching process during fabrication. In the optical microscopy (OM) image in Figure 12c, our metasurface absorber can be differentiated from the areas with only TiN film, the bottom layer of the absorber. In the optical measurements, white light source impinged on the absorber from the top of the sample and the absoprtion (A) is calculated by measuring the reflection (R) and transmission (T) via the relation of A=1-R-T.

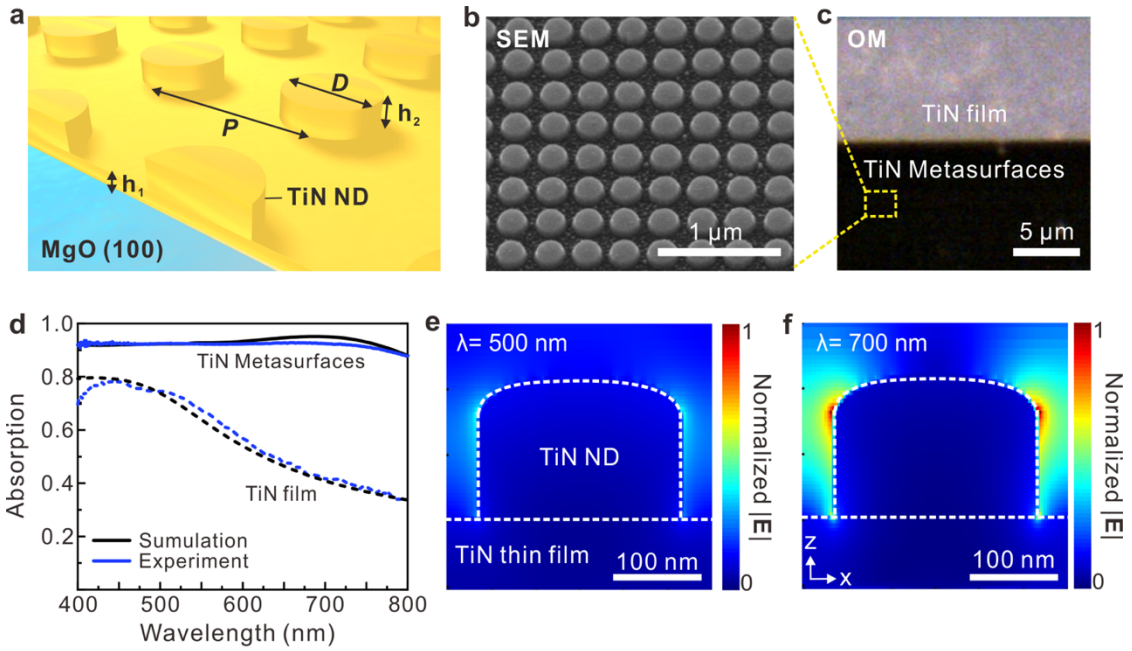

Figure 12. Plasmonic perfect absorber using the TiN metasurface. a) Schematic of the broadband plasmonic perfect absorber that contains TiN nanodisk arrays on a 50-nm TiN thin film. The geometric parameters of the TiN nanodisk arrays are P= 310 nm, D= 230 nm, and h_2= 110 nm. b) Tilted SEM image of the TiN metasurface. c) OM image of the TiN film and TiN metasurfaces. d) Measured (blue) and calculated (black) absorption spectra of the TiN metasurface (solid) and 160-nm TiN film (dashed). e) Normalized electric field profile of the unit cell (a TiN nanodisk on TiN film) at λ= 500 nm excited by a normally incident plane wave. f) Normalized electric field profile of the unit cell at λ= 700 nm showing a strong LSPR.

With the screened plasma frequency $\omega_{ps}(\cong 2.43\, eV \cong 510\, nm)$ located in the visible frequency range (permitivity goes to zero), the absorption spectrum in Figure 12d can be separated in terms of $\mathrm{Re}(\varepsilon)$ versus wavelength λ into two parts. The first part is in the region of $\lambda < 510\ \mathrm{nm}$, where $\mathrm{Re}(\varepsilon) > 0$ and TiN acts as a lossy dielectric material; the second part is in the range of $\lambda > 510\ \mathrm{nm}$,

in which $\mathrm{Re}(\varepsilon) < 0$ and TiN function as a metal. First, we analyzed the 160-nm TiN film spectrum (dashed lines in Figure 12d). The high absorption feature close to the short-wavelength range of $\lambda < 510\ \mathrm{nm}$ can be explained by the intrinsic absorption - a strong broad interband transition — associated with the previous discussion on $\mathrm{Im}(\varepsilon)$, while for the long-wavelength range of $\lambda > 510\ \mathrm{nm}$, the metallic property of TiN prevents incident light from penetrating through the bulk, thereby causing high reflection and low absorption in the long-wavelength (low photon energy) range. In contrast to the 160-nm TiN film, our metasurface absorber (solid lines in Figure 12d) demonstrates an experimentally averaged absorption as high as 92% over the visible range from 400 nm to 800 nm as a result of contributions from the localized plasmonic resonance.

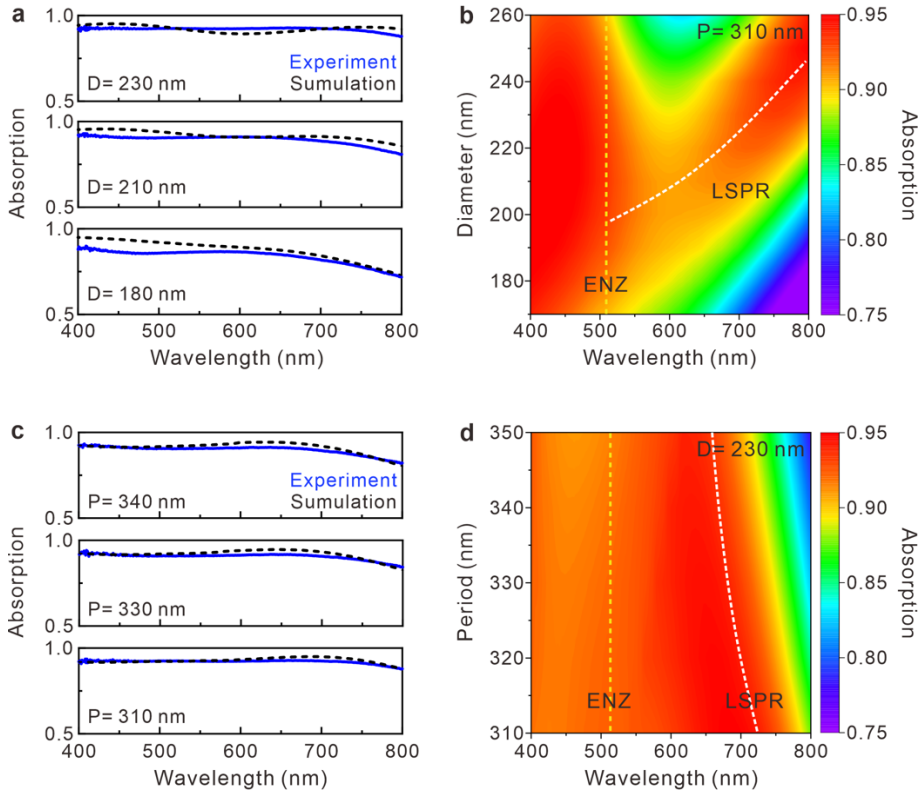

Figure 13. Diameter-dependent and periodicity-dependent absorption spectra of the TiN metasurface. a) experimentally measured (blue) and numerically calculated (black) absorption spectra from TiN metasurface with varied diameter of the TiN nanodisk arrays and fixed periodicity of P= 310 nm. b) Color map of numerically calculated absorption spectra as a function of the diameter of the TiN nanodisk arrays with fixed periodicity of P= 310 nm. c) experimentally measured (blue) and numerically calculated (black) absorption spectra from TiN metasurface with varied periodicity of the TiN nanodisk arrays with a fixed diameter of D= 230 nm. d) Color map of numerically calculated absorption spectra as a function of periodicity of the TiN nanodisk arrays with a fixed diameter of D= 230 nm.

The resonance peak position can be manipulated by changing the size of the structures, a spectral tunability that is used to optimize the broadband absorption. As shown in Figure 13, the geometric mappings obtained by sweeping the diameter (D) and periodicity (P) of the nanodisk arrays in experiments and simulations confirm that absorption peaks from the LSPR contribution shift when the configuration changes. In the simulation of Figure 13a, the absorption peak at $\lambda > 510\ \mathrm{nm}$ undergoes a spectral redshift with increasing D. This change leads to a decrease in the absorption at approximately 600 nm when D increases from 230 nm to 260 nm. Therefore, to maintain an average high absorption, the diameter of our design is set to 210 nm. Similar trends appear

between the simulation and experimental measurements with slight discrepancy due to fabrication imperfections and measurement noise in short-wavelength ranges. The simulation outcome when sweeping the periodicity, as illustrated in Figure 13c, implies that the broadband absorption becomes narrower with increasing P. In the plasmonic regime of $\lambda > 510\ \mathrm{nm}$, when P increases, the absorption peak slightly shifts toward the short-wavelength region. As demonstrated (Figure 13c), the configuration with a periodicity of 310 nm possesses the optimized broadband absorption, which agrees with the simulation results in Figure 13d.

In summary, we theoretically calculated and experimentally demonstrated a refractory metamaterial perfect absorber that exhibits broadband perfect absorption in the visible region using a TiN metasurface. The structure contains TiN nanodisk array metasurfaces on a TiN thin film. Notably, our ultrathin all-TiN metasurface perfect absorber simplifies the fabrication processes compared with other MIM-based TiN nanostructured absorbers. The demonstration of a refractory plasmonic perfect absorber with a broadband LSPR provides a new approach for realizing solar-energy-related and solar thermophovoltics.

1.3. Communities of Interest:

Before the COVID-19 pandemic, our group and SPIE Student Chapter at Baylor University participated Waco STEM Family Night to promote optics to the local elementary schools. We showcased various hands-on demonstrations with simple and interesting photonic topics. In addition, we also showed fabricated TiN samples as one of the demonstrations to show the control of optical properties (e.g. absorption) using TiN thin films. More than **1000 visitors** attended and having fun with simple optics demonstrations (Fig. 14). They also get to know bit of knowledge on optical alignment and nano-optical structures.

Figure 14. Outreach activities and exhibition for Waco STEM Family Night during February 2020.

2. Impact:

Our work enriches the fundamental understanding of emission and absorption properties on TiN ENZ and plasmonic materials and nanostructures that could be important for the development of advanced nanoscale lasers/light sources, high-temperature applications such as solar thermophovoltics, optical/bio-sensors, and nano-optoelectronic devices. In addition, the

fabrication techniques of high quality TiN ENZ/plasmonic materials will also be important for future investigation of ENZ/plasmonic metasurfaces and nano-devices.

Furthermore, through this project, our U.S. team and TW team have established a close collaboration, including exchanging TiN samples, sharing optical measurement data, and discussing results. The students in PI groups had also actively involved in the discussion and planning of this international collaborative project. Sixteen journal papers were published/submitted including two joint papers, and more than 20 conference invited talks were presented during the grant period. PIs and their students also earned prestigious awards during the grant period. This project provided a solid foundation for research collaboration on ENZ/plasmonic optics based on high-quality TiN thin films and opened future research opportunites.

References

[1] J. W. Christopher, B. B. Goldberg, and A. K. Swan, "Long tailed trions in monolayer MoS_2: Temperature dependent asymmetry and resulting red-shift of trion photoluminescence spectra," (in English), *Scientific Reports,* Article vol. 7, p. 14062, Oct 2017, Art no. 14062, doi: 10.1038/s41598-017-14378-w.

[2] N. Danz, R. Waldhausl, A. Brauer, and R. Kowarschik, "Dipole lifetime in stratified media," (in English), *Journal of the Optical Society of America B-Optical Physics,* Article vol. 19, no. 3, pp. 412-419, Mar 2002, doi: 10.1364/josab.19.000412.

[3] K. A. Neyts, "Simulation of light emission from thin-film microcavities," (in English), *Journal of the Optical Society of America a-Optics Image Science and Vision,* Article vol. 15, no. 4, pp. 962-971, Apr 1998, doi: 10.1364/josaa.15.000962.

[4] P. Bharadwaj and L. Novotny, "Spectral dependence of single molecule fluorescence enhancement," *Opt Express,* vol. 15, no. 21, pp. 14266-14274, 2007/10/17 2007, doi: 10.1364/OE.15.014266.

[5] M. Amani *et al.*, "Near-unity photoluminescence quantum yield in MoS2," (in English), *Science,* Article vol. 350, no. 6264, pp. 1065-1068, Nov 2015, doi: 10.1126/science.aad2114.

[6] S. S. Kharintsev, A. V. Kharitonov, A. R. Gazizov, and S. G. Kazarian, "Disordered Nonlinear Metalens for Raman Spectral Nanoimaging," *ACS Applied Materials & Interfaces,* vol. 12, no. 3, pp. 3862-3872, 2020/01/22 2020, doi: 10.1021/acsami.9b19555.

[7] W. A. Britton, Y. Chen, and L. Dal Negro, "Double-plasmon broadband response of engineered titanium silicon oxynitride," *Opt. Mater. Express,* vol. 9, no. 2, pp. 878-891, 2019/02/01 2019, doi: 10.1364/OME.9.000878.

[8] E. Shkondin, T. Repän, O. Takayama, and A. V. Lavrinenko, "High aspect ratio titanium nitride trench structures as plasmonic biosensor," *Opt. Mater. Express,* vol. 7, no. 11, pp. 4171-4182, 2017/11/01 2017, doi: 10.1364/OME.7.004171.

[9] L. Braic *et al.*, "Titanium Oxynitride Thin Films with Tunable Double Epsilon-Near-Zero Behavior for Nanophotonic Applications," *ACS Applied Materials & Interfaces,* vol. 9, no. 35, pp. 29857-29862, 2017/09/06 2017, doi: 10.1021/acsami.7b07660.

[10] A. Kharitonov and S. Kharintsev, "Tunable optical materials for multi-resonant plasmonics: from TiN to TiON [Invited]," *Opt. Mater. Express,* vol. 10, no. 2, pp. 513-531, 2020/02/01 2020, doi: 10.1364/OME.382160.

3. Publications and presentations (accumulated from the project start date)

Published/submitted journal articles:

1. J. Yang, S. Gurung, S. Bej, P. Ni, **H.W.H. Lee***, "Active Optical Metasurfaces: Comprehensive Review on Physics, Mechanisms, and Prospective Applications" accepted in ***Reports on Progress in Physics*** (2021)
2. R. Mishra, C.-W. Chang, A. Dubey, Z.-Y. Chiao, T.-J. Yen, **H.W.H. Lee**, Y.-T. Lu, and **S. Gwo**,* "Optimized titanium nitride epitaxial film for refractory plasmonics and solar energy harvesting," accepted in ***J. Phys. Chem. C*** *125, 13658* (2021).
3. K. Minn, A. Anopchenko, Y.-J. Lu, C.-W. Chang, R. Mishra, J. Kim, Z. Zhang, **S. Gwo**, and **H.W.H. Lee**,* "Enhanced spontaneous emission of monolayer MoS_2 on epitaxially grown titanium nitride epsilon-near-zero thin films," ***Nano Letter*** 21, 4928 (2021).
4. M. J. Yu , C.L. Chang , H.Y. Lan , Z.Y. Chiao , Y.C. Chen , **H.W.H. Lee**, Y.C. Chang, S.W. Chang, T. Tanaka, V. Tung , H.H. Chou, and Y.J. Lu, "Plasmon-Enhanced Solar-Driven Hydrogen Evolution Using Titanium Nitride Metasurface Broadband Absorbers" ***ACS Photonics*** 8, 3125 (2021)
5. Y. Sang, C.-Y. Wang, S. S. Raja, C.-W. Chang, C.-T. Huang, C.-A. Chen, X.-Q. Zhang, H. Ahn, C.-K. Shih, Y.-H. Lee, J. Shi, and **S. Gwo**,* "Tuning of two-dimensional plasmon–exciton coupling in full parameter space: A polaritonic non-Hermitian system," ***Nano Letter.*** vol. 21, pp. 2596–2602 (2021).
6. C.-Y. Wang, Y. Sang, X. Yang, S. S. Raja, C.-W. Cheng, H. Li, Y. Ding, S. Sun, H. Ahn, C.-K. Shih,* **S. Gwo**,* and J. Shi,* "Engineering giant Rabi splitting via strong coupling between localized and propagating plasmon modes on metal surface lattices: observation of sqrt(*N*) scaling rule," ***Nano Lett.*** vol. 21, pp. 605–611 (2021).
7. C.-W. Cheng, S. S. Raja, C.-W. Chang, X.-Q. Zhang, P.-Y. Liu, Y.-H. Lee, C.-K. Shih, and **S. Gwo**,* "Epitaxial aluminum plasmonics covering full visible spectrum," ***Nanophotonics*** vol. 10, pp. 627–637 (2021).
8. S. S. Raja, C.-W. Cheng, and **S. Gwo**,* "Low-loss aluminum epitaxial film for scalable and sustainable plasmonics: Direct comparison with silver epitaxial film," ***Nanoscale*** vol. 12, pp. 23809–23816 (2020).
9. A. Dubey, R. Mishra, Y.-H. Hsieh, C.-W. Cheng, B.-H. Wu, L.-J. Chen, **S. Gwo**,* and T.-J. Yen,* "Aluminum plasmonics enriched ultraviolet GaN photodetector with ultrahigh responsivity, detectivity, and broad bandwidth," ***Adv. Sci.*** 2002274 (2020).
10. S. S. Raja, C.-W. Cheng, Y. Sang, C.-A. Chen, X.-Q. Zhang, A. Dubey, T.-J. Yen, Y.-M. Chang, Y.-H. Lee, and **S. Gwo**,* "Epitaxial aluminum surface-enhanced Raman spectroscopy substrates for large-scale 2D material characterization," ***ACS Nano*** vol. 14, pp. 8838–8845 (2020).
11. W.-P. Guo, W.-Y. Liang, C.-W. Cheng, W.-L. Wu, Y.-T. Wang, Q. Sun, S. Zu, H. Misawa, P.-J. Cheng, S.-W. Chang, H. Ahn,* M.-T. Lin,* and **S. Gwo**,* "Chiral second-harmonic generation from monolayer WS_2/aluminum plasmonic vortex metalens," ***Nano Lett.*** vol. 20, pp. 2857–2864 (2020)
12. A. Anopchenko, S. Gurung, S. Bej, and **H. W. Lee**, "Field Enhancement of Epsilon-near-Zero Modes in Realistic Ultra-Thin Absorbing Films", submitted to *Physical Review Letter* (2021).
13. A. Anopchenko, S. Bej, N. Danz, G. S. Agarwal and **H. W. Lee**, "Active Light Emission Control via Tunable Hybrid Plasmon Polariton Mode", to be submitted to *Optics Express* (2021)
14. W.-P. Guo, R. Mishra, C.-W. Cheng, B.-H. Wu, L.-J. Chen, M.-T. Lin, and **S. Gwo**,* "Titanium nitride epitaxial films as an alternative plasmonic material platform: beyond gold in the visible range," *ACS Photonics* 6. 1848 (2019).

15. L. Sun, C.-Y. Wang, A. Krasnok, J. Choi, J. Shi, J. S. Gomez-Diaz, A. Zepeda, **S. Gwo**, C.-K. Shih, A. Alù,* and X. Li,* "Separation of valley excitons in a MoS_2 monolayer using a subwavelength asymmetric groove array," *Nature Photonics* vol. 13, pp. 180–184 (2019).

16. F. Cheng, C.-J. Lee, J. Choi, C.-Y. Wang, Q. Zhang, H. Zhang, **S. Gwo**, W.-H. Chang, X. Li, C.-K. Shih,* "Epitaxial growth of optically thick, single crystalline silver films for plasmonics," *ACS Appl. Mater. Interfaces* vol. 11, pp. 3189–3195 (2019).

17. S. K. Rai, K.-W. Kao, **S. Gwo**, A. Agarwal, W. D. Lin, and J. A. Yeh,* "Indium nitride (InN)-based ultrasensitive and selective ammonia sensor using an external silicone oil filter for medical application," *Sensors* vol. 18, 3887 (2018).

18. J. Shi, W.-Y. Liang, S. S. Raja, Y. Sang, X.-Q. Zhang, C.-A. Chen, Y. Wang, X. Yang, Y.-H. Lee,* H. Ahn,* and **S. Gwo**,* "Plasmonic enhancement and manipulation of optical nonlinearity in monolayer WS_2," *Laser Photonics Reviews* vol. 12, 1800188 (2018).

Conference talks:

1. S. Gurung, K. Minn, A. Anopchenko, S. Bej, **H. W. Lee**, "Enhancement of Optical Nonlinearity and Spontaneous Emission in Nano-engineered Epsilon-Near-Zero Materials", *SPIE Optics + Photonic Conference 2021*, San Diego, USA (Virtual) (August 2021) (Invited).
2. **H. W. Lee**, "Active Epsilon-Near-Zero (ENZ) photonics", 1st Colloquium on the Physics and Applications of Metasurfaces", France (Virtual) (June 2021) (Invited).
3. S. Gurung, K. Minn, A. Anopchenko, S. Bej, **H. W. Lee**, "Enhancement of Optical Nonlinearity and Spontaneous Emission in Nano-engineered Epsilon-Near-Zero Materials", *SPIE Optics + Photonic Conference 2021*, San Diego, USA (August 2021). (Invited).
4. **H. W. Lee**, A. Anopchenko, S. Gurung, K. Minn, J. Yang, "Active Epsilon-Near-Zero Photonics", *International Conference on Metamaterials, Photonic Crystals and Plasmonics (META 2020)*, (Virtual) (July 2021) (Keynote).
5. **H. W. Lee**, "Linear and nonlinear conducting oxide epsilon-near-zero nanophotonics", 2020 Materials Research Society (MRS) Fall Meeting (December 2020) (Invited).
6. **H. W. Lee**, "Enhanced optical nonlinearity and emission in atomically engineered epsilon-near-zero materials", *2020 OSA Optics and Photonics Congresses: Advanced Photonics*, *Novel Optical Materials and Application Topical Meeting (NOMA),* Zurich, Switzerland, (July 2020) (Invited).
7. A. Anopchenko, K. Minn, S. Bej, S. Gurung, and **H. W. Lee**, "Enhanced Quantum Emission and Molecular Detection in Epsilon-near-zero Meta-structures", *SPIE Photonic West Conference 2020*, San Francisco (February 2020) (Invited).
8. S. Gurung, J. Yang, A. Anopchenko, S. Bej, K. Minn, **H. W. Lee**, "Epsilon-near-zero Optics in Planar and Optical Fiber Platform", *50th Winter Colloquium on the Physics of Quantum Electronics (PQE 2020)*, Utah, USA (January 2020) (Invited).
9. A. Anopchenko, S. Gurung, S. Bej, J. Joyner, **H. W. Lee**, "Field Enhancement of Epsilon-near-Zero Modes in Atomic-Layer-Deposited ZnO:Al Nanolayers", *IEEE Photonics Conference 2019,* San Antonio, USA (September 2019).
10. S. Gurung, A. Anopchenko, S. Bej, J. Yang, **H. W. Lee**, "Gate-tunable epsilon-near-zero Meta-structures", *SPIE Optics + Photonic Conference 2019*, San Diego, USA (August 2019) (Invited).
11. A. Anopchenko, S. Bej, S. Gurung, K. Minn, J. Yang, **H. W. Lee**, "Gate-tunable Conducting Oxide Epsilon-near-zero Metasurfaces with Active Nonlinear and Quantum Responses", *International Conference on Metamaterials, Photonic Crystals and Plasmonics (META 2019)*, (June 2019) (Invited).
12. S. Gurung, A. Anopchenko, S. Bej, J. Yang, **H. W. Lee**, "Electronically-tunable Conducting Oxide Epsilon-near-zero Heterostructures", *The 9th International Multidiscipline Conference on Optofluidics (IMCO2019),* Hong Kong (June 2019) (Invited).

13. A. Anopchenko, S. Bej, S. Gurung, J. Yang, L. Tao, C. Arndt, **H. W. Lee**, "Tunable conducting oxide epsilon-near-zero meta-devices", *SPIE Photonic West Conference 2019*, San Francisco (February 2019) (Invited).
14. **S. Gwo,** Materials Research Meeting 2019 (MRM2019), Symposium G-4: Plasmonic Materials: from Fundamentals to Applications, Yokohama, Japan, December 10–14, 2019 (Invited).
15. **S. Gwo,** 2019 MRS Fall Meeting, Symposium EL01: Emerging Material Platforms and Approaches for Plasmonics, Metamaterials and Metasurfaces, Boston, USA, December 1–6, 2019 (Invited).
16. **S. Gwo,** The 2nd International Conference on SERS (SERS-2019), Suzhou, China November 6–9, 2019 (Keynote).
17. **S. Gwo,** The Batsheva de Rothschild and Israel Science Foundation Seminar on Nonlinear Metamaterials and Photonic Crystals, Kfar Blum, Israel, September 9–12, 2019 (Invited).
18. **S. Gwo,** The XXVIII International Materials Research Congress, Symposium A1: Nanostructured Plasmonic Materials, Cancun, Mexico, August 18–23, 2019 (Invited).
19. **S. Gwo,** SPIE Nanoscience + Engineering 2019, Conference on "Plasmonics: Design, Materials, Fabrication, Characterization, and Applications XVII," San Diego, USA, August 11–15, 2019 (Invited).
20. **S. Gwo,** META 2019 Conference (The 10th International Conference on Metamaterials, Photonic Crystals and Plasmonics), Lisbon, Portugal, July 23–26, 2019 (Invited).
21. **S. Gwo,** Symposium on Surface and Nano Science 2019 (SSNNS'19), Shizukuishi, Iwate, Japan, January 14–18, 2019 (Invited).

Invited Seminars at Universities:

- **Howard Lee**, Rice University (April 2021)
- **Howard Lee**, Boston University (March 2020)
- **Howard Lee**, Virginia Commonwealth University (November 2019)
- **Howard Lee**, UC Irvine (October 2019)
- **Howard Lee**, IEEE Photonics Chapter, San Diego (October 2019)
- **Howard Lee**, Academia Sinica. Taiwan (September 2019)
- **Howard Lee**, National Cheng Kung University, Taiwan (September 2019)
- **Howard Lee**, TexasA&M (April 2019)
- **Howard Lee**, Texas Tech University (Nov 2018)
- **Howard Lee**, TexasA&M Commerce (Oct 2018)

Awards:

- **Howard Lee,** 2020 SPIE Rising Researcher
- **Howard Lee**, 2020 Baylor Outstanding Faculty
- **Howard Lee**, 2019 DARPA Director's Fellowship
- **Howard Lee**, Young Scientist Award, 2019 Optoelectronic Global Conference
- **Howard Lee**, 2019 OSA Senior Member
- **Shangjr Gwo**, The 23rd National Chair Professorship, Ministry of Education, Taiwan (2019)